Supplementary Material

Room-temperature photoconductivity in superconducting tungsten meander wires

Abhishek Kumar,[a,b] Alka Sharma,[c] Animesh Pandey,[a,b] M.P. Saravanan,[d] Sudhir Husale[a,b]*

[a]CSIR-National Physical Laboratory, Dr. K. S. Krishnan Marg, New Delhi-110012, India.

[b]Academy of Scientific and Innovative Research (AcSIR), Ghaziabad- 201002, India.

[c]Tohoku University, Department of Materials Processing, Sendai, Japan.

[d]Low Temperature Laboratory, UGC-DAE Consortium for Scientific Research, University Campus, Khandwa Road, Indore 452001, India.

**Corresponding Author- husalesc@nplindia.org*

S1 Section: A schematic view of focused ion beam (FIB) technique setup and TEM analysis of FIB fabricated meander structured tungsten (MW) wires.

The MW wires were fabricated on SiO_2/Si substrate using FIB technique, for this a schematic view of used FIB instrument setup is shown in Fig. S1. In the Fig. S1, the mentioned gallium ion (Ga^+) beam and FIB-assisted gas injection system (GIS) having hexamethyl carbonyl tungsten [$W(CO)_6$] precursor are in-situ used for deposition of tungsten (W) films in the required dimension on particular region on the substrate. Further, the Ga^+ beam is again used for the milling with controlled scanning on W films to structure the meander wires with the application of FIB equipped scanning electron microscope tool. This control process of fabrication results the novel structuring of MW wires of different width and areas. Also, we have shown an optical image of FIB fabricated MW device on substrate, wherein the electrical connections are made in four-probe configurations to the gold (Au) pads from the MW wires. For FIB deposited tungsten samples, the performed Raman measurements shown in below Fig. S1(b), indicate the presence of tungsten carbide (WC) stretching modes to the corresponding peaks of 678.6 cm^{-1} and 789.9 cm^{-1}. Note that the Raman spectra for two MW (MW1, MW3) is same, accordingly same nature we believe that for other MW samples also. The marked peaks 'S' signals are from the substrate as we have compared this data with SiO2/Si substrate (black curve). Also, Fig. S1(c) shows the HRTEM images at 10 nm scale for FIB deposited W, which exhibits its polycrystalline nature with the presence of lines (lattice fringes), defects, and amorphous regions, which are marked in circles. Further, for confirmation we need XRD pattern for the W for the identification of phase/plane information, lattice (d) spacing, which couldn't realize due to some instrumental limitations for the time being.

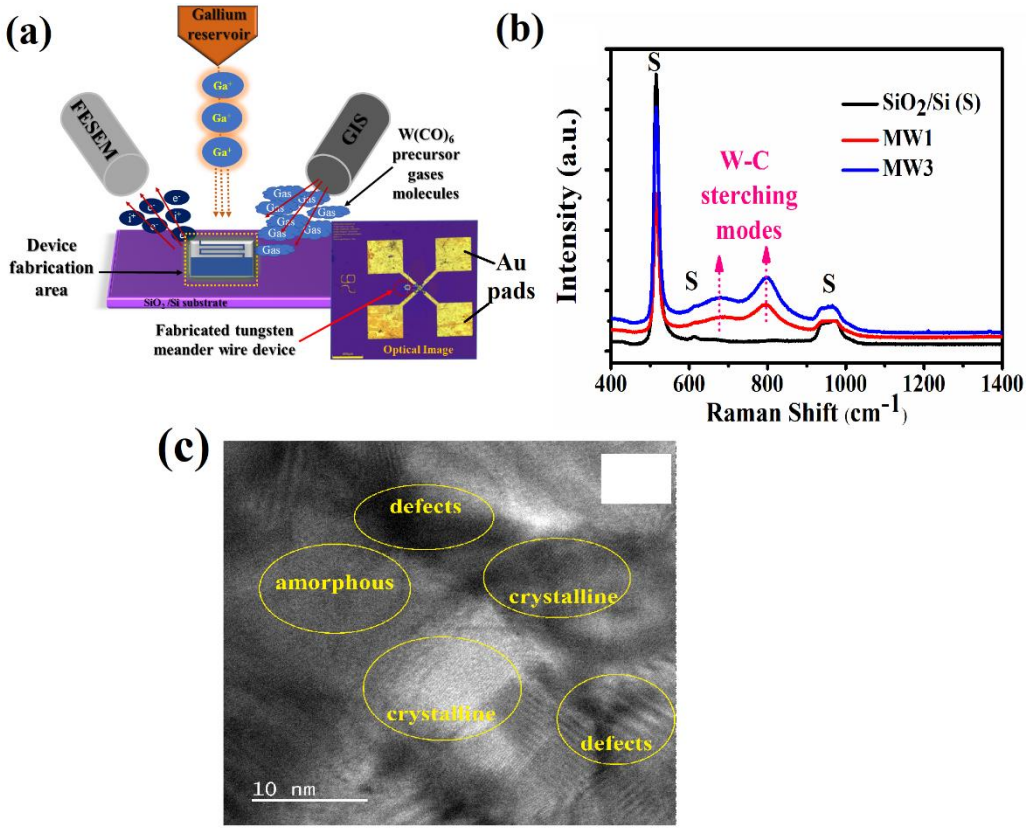

Figure S1. (a) A schematic view of the FIB instrument setup- equipped with gallium ion beam, $W(CO)_6$ gas precursor in gas injection system and FIB-assisted an electron microscope for SEM imaging. **(b)** The obtained Raman spectrum of MW samples, represents WC stretching modes for FIB deposited W. **(c)** HRTEM images at 10 nm, which shows the crystallinity nature of the MW wires.

S2 Section: Room-temperature photoresponse measurements on MW1 wire with the illumination of laser light of 532 nm wavelength (visible region) at the fixed power of 486 mW/cm^2 after six months.

For the evaluation of stability features of MW (MW1) wires, we have performed the 532 nm laser light (of fixed power 486 mW/cm^2) dependent photoresponse measurements on MW1 wire after six months at the room temperature (300 K). We have measured the time dependent rise and decay in current with the presence (ON state) and absence (OFF state) of laser light respectively. In results, the Fig. S2(a) display the behaviour of photocurrent (I_{ph}) as a function of time, which were measured with the applied fixed voltages of values 100 mV, 500 mV, 700 mV, and 1 V for the MW1 wire. From the Fig. S2(a), it is clear that the observed I_{ph} rises as we increase the applied fixed voltages. We have extracted the maximum I_{ph} values for these fixed voltages, which are plotted in inset of Fig. S2(b) as a function of voltage. The linear increment of I_{ph} with the voltages is confirmed by the well-fitted red curve of linear equation. Further, for the evaluation of photoresponse performance of FIB fabricated MW1 wire, we have extracted the critical parameters like-, photoresponsivity (R_{ph}), detectivity (D) and external quantum efficiency (E.Q.E) using eqn.s 1, 2 and 3 respectively (mentioned in the main description of paper). We have calculated the highest R_{ph} and D values of 8.7 A/W and 12.9

$\times 10^6$ Jones and further E.Q.E of 20.28 % for MW1 wire for the applied highest voltage value of 1 V under the illumination 532 nm wavelength laser light. The extracted R_{ph} and D values are plotted as a function of bias voltages in the main panel of Fig. S2(b) using double Y-axis, both (R_{ph} and D) increases in linear manner approximately with the increment of bias voltages. Further, we have plotted the one ON-OFF cycle of 1V- generated behaviour of I_{ph} as a function of measuring time (shown in black curve) in Fig. S2(c) for the MW1 wire. Further, we have fitted this data using eqn.s 4 and 5 for the evaluation of rise time (τ_r) for ON region and decay time (τ_d) for OFF region respectively which are in well agreement with the experimental data, shown by the pink colour curve and light green colour for τ_r and τ_d respectively. The fitted value of τ_r and τ_d are found of 1235 millisecond and 789 milliseconds respectively for MW1 wire. The calculated values of rise time and decay time is higher than the earlier measured (before six months) for MW1 wire, indicated the slight degradation in generation of charge carriers but significant capability for exhibiting the well photoresponse features even after six months.

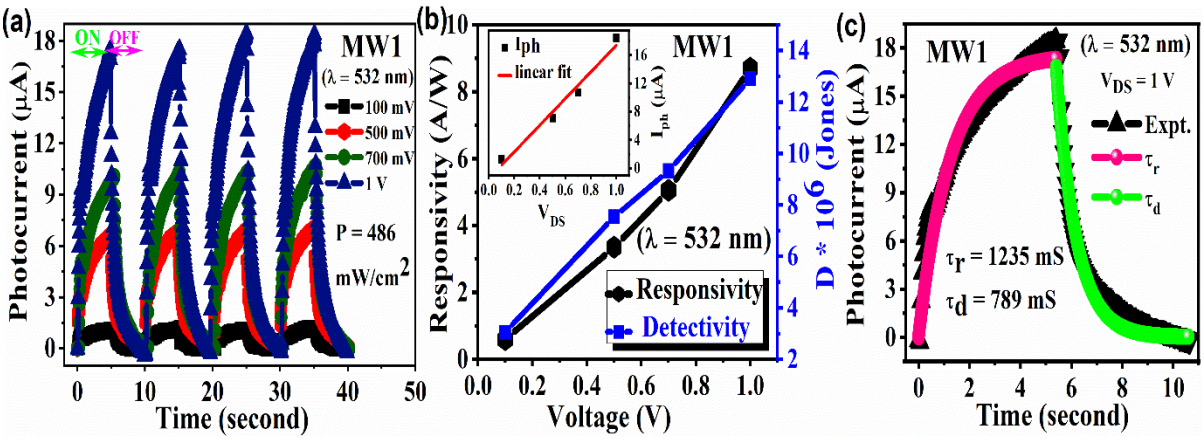

Fig. S2 The room temperature photoresponse results for MW1 wire under the illumination of 532 nm laser light (of visible region) at the fixed power 486 mW/cm^2.

S3 Section: Room-temperature photoresponse measurements on MW1 wire with the illumination of laser light of wavelength 1064 nm (NIR region) at the fixed power of 18 mW/cm^2 after six months.

Fig. S3 shows the photoresponse characteristics for the MW1 wire under the illumination of laser light of near infrared region (1064 nm) at fixed power of 18 mW/cm^2. Fig. S3(a) shows the I_{ph} characteristics as a function of time, which is measured at fixed applied voltages of values 100 mV, 500 mV, 700 mV, and 1 V for MW1 wire. Further, the extracted maximum I_{ph} values are plotted in inset of Fig. S3(b) as function of voltage, which is further fitted with linear equation. The well agreement of linear fitting (red curve) on I_{ph} concluded the its linear increment with the applied bias voltages. Further, with the data of Fig. S3(a), we have extracted the voltages dependent values of responsivity (R_{ph}) and detectivity (D) using eqn.s 1 and 2 (mentioned in manuscript) respectively. The values of R_{ph} and D are plotted in the main panel

of Fig. S3(b) as a function of voltage using double y-axis, which state that the values of R_{ph} and D also increases with the increment of applied voltages. We have calculated the highest R_{ph} and D values of 10.92 A/W and 16.2 $\times 10^6$ Jones and further E.Q.E of 12.72 % is estimated using eqn. 3 for MW1 wire for the applied highest voltage value of 1 V. Here, we noted that the R_{ph} value at 1V for MW1 is lower with the illumination of 532 nm laser light in comparison to 1064 nm laser light, which can be related with the power density of illuminated laser light. Since, from the eqn. 1, it is clear that the R_{ph} is anti-proportional to the power density, which results in lower responsivity for MW1 wire under the illumination of 532 nm laser light at the high power of 486 mW/cm^2 in comparison to 1064 nm laser light at the low power of 18 mW/cm^2. Further, we have plotted the 1V- generated I_{ph} characteristics (from Fig. S3(a)) as a function of measuring time in Fig. S3(c) only for one ON-OFF cycle (black curve) for the MW1 wire. Using eqn.s 4 and 5, we have fitted this one I_{ph} cycle for the evaluation of τ_r and τ_d respectively which is in the well agreement with the experimental data, shown by the pink colour curve and light green colour curve for τ_r and τ_d respectively as shown in Fig. S3(c). The fitted value of τ_r and τ_d are of 1286 millisecond and 718 milliseconds respectively for MW1 wire. The value of rise time is also higher than the decay time for MW1 wire under the illumination of 1064 nm laser light. Similarly, these results of τ_r and τ_d are higher than earlier measured under the illumination of 1064 nm laser light for MW1 wire. Thus, these photoresponse features for MW1 wires after six months results significant capability for the applicability in optoelectronics application for a long time.

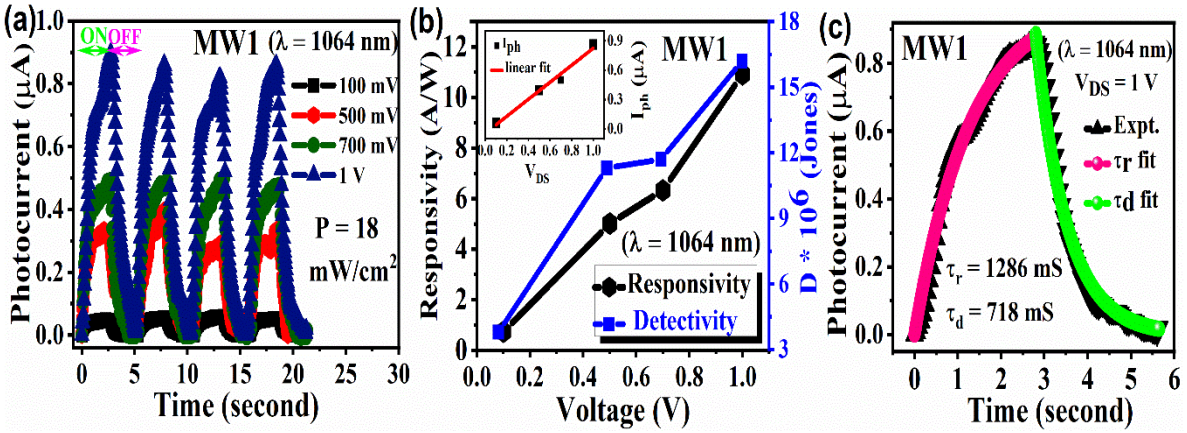

Fig. S3 The photoresponse characteristics of MW1 wire under the illumination of 1064 nm laser light (of near infrared region) at the fixed power 486 mW/cm^2.

S4 Section: Room-temperature photoresponse measurements on MW1 wire with power variation of 1064 nm illuminated laser light (of NIR region) after six months.

Furthermore, we have also evaluated photoresponse features with fixed voltage of 500 mV for MW1 wire with the power density variation ranging from 6 mW/cm^2 to 18 mW/cm^2 of

illuminated 1064 nm laser light, which are plotted in Fig. S4(a). We clearly see the enhancement of I_{ph} with the rise in power density of 1064 nm laser light which suggest that the higher charge carrier generation with the higher power intensity. Using R_{ph} relation (eqn. 1), we have extracted the R_{ph} values with the data of Fig. S4(a), which are plotted in Fig. S4(b) as a function of power using double Y-axis wherein on the other Y-axis the I_{ph} values have been taken. From the Fig. S4(b) it is clear that the measured I_{ph} and R_{ph} is rises with the increase of power densities which suggest that the densities of available state in energy gap increased under the high-power laser densities, and hence cause the enhancement of I_{ph} and R_{ph}. Herein, the I_{ph} is fitted with the relation $I \sim P^{\theta}$ and fitting is shown with solid red line. Here, the obtained value of $\theta > 1$, represents the defects states across the channel of the samples. Thus, here we have concluded the significant features of MW1 wire with power variation of illuminated 1064 nm laser light.

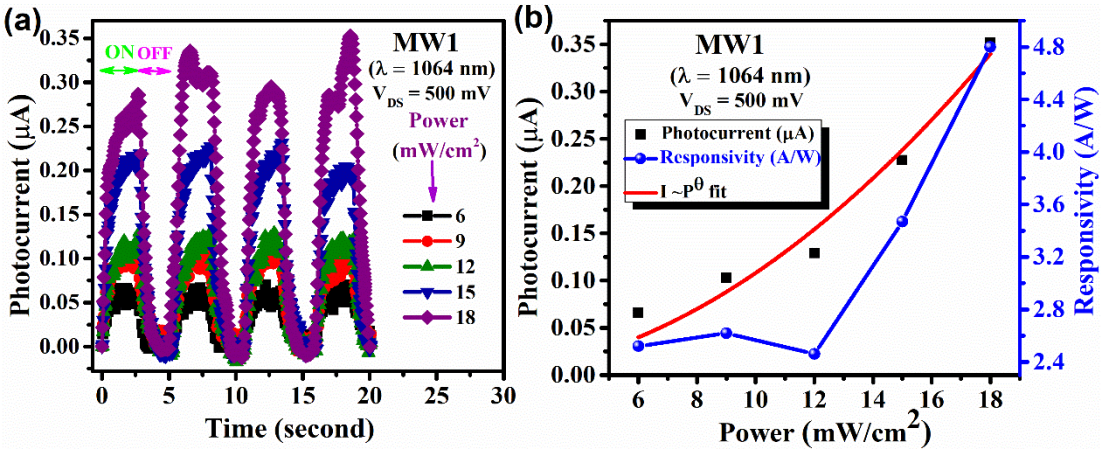

Fig. S4 The power density dependent dynamics of photoresponse measurements for MW1 wire under the illumination of 1064 nm laser light (of near infrared region) at room-temperature (300 K).

S5 Section: The comparison of photoresponse measurements on MW1 wire under the illumination of different light (laser) sources such as- Halogen light, 532 nm, 1064 nm, 1550 nm at room-temperature.

Herein, we have compared the obtained photocurrent (I_{ph}) characteristics for MW1 wire under the illumination of different sources such as- Halogen light, and lasers- 532 nm, 1064 nm, 1550 nm wavelengths. We clearly see that the I_{ph} is decrease with the increment of wavelength of laser light as incident (illumination) energy decreases. For halogen light, the I_{ph} is less than the 532 nm, this may be because of lower power density of light sources in compare to 532 nm laser. Note that these measurements were performed after approx. 1 year, so because of this we are getting the lower I_{ph} values in comparison to earlier measured. Thus, these results show the significant stability of FIB fabricated W- devices for optoelectronics applications with Broadspectral range of photoresponse

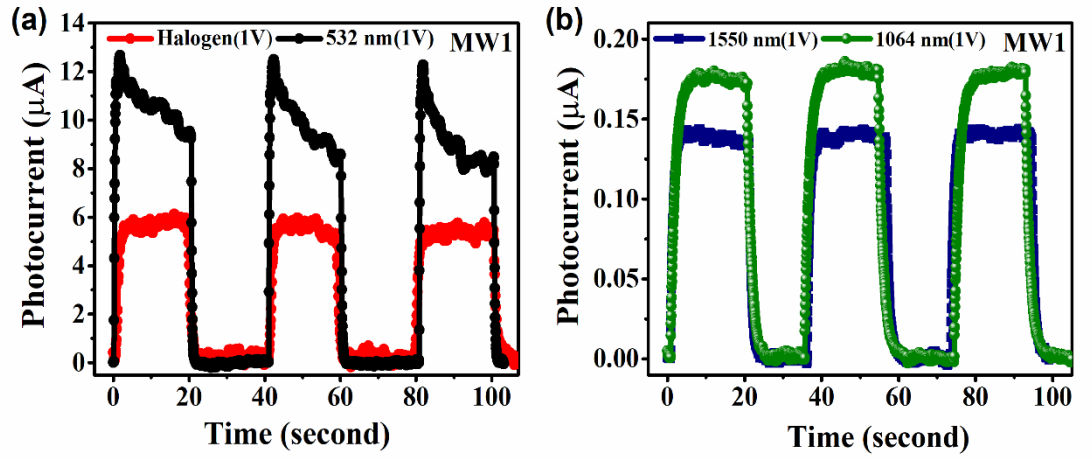

Fig. S5 The comparison of photocurrent under different light sources such as- Halogen light, and 532 nm, 1064 nm, 1550 nm wavelengths laser for MW1 wire.